Pressure-induced distortions of $Pb(NO_3)_2$ isomorphs

Robert R. Winters and William S. Hammack*
Department of Chemical Engineering, Carnegie-Mellon University, Pittsburgh, Pennsylvania 15213-3890
(Received 27 November 1995)

Energy-dispersive and angle-dispersive x-ray-diffraction (EDXD and ADXD) measurements show that when compressed by pressures above 10.0 GPa isostructural $Pb(NO_3)_2$, $Ba(NO_3)_2$, and $Sr(NO_3)_2$ transform reversibly to highly disordered structures. Raman measurements under compression suggest that the transformation occurs via reorientation of the nitrate ions to multiple sites and movement of the metal ions from the crystal positions. Our main conclusion is that EDXD and ADXD measurements give different meanings to the notion ''x-ray amorphous.'' Thus, whenever this phrase is used, the method used and the conditions that prevail must be specified. We also suggest that our results show that Raman spectroscopy can be used to distinguish nonrandom nitrate and cation environments in metal nitrate glasses. [S0163-1829(96)05821-3]

I. INTRODUCTION

In this paper we report the effect of high hydrostatic pressures on a series of crystals with structures isomorphic to $Pb(NO_3)_2$. Our initial energy-dispersive x-ray-diffraction (EDXD) measurements showed that $Pb(NO_3)_2$, $Ba(NO_3)_2$, and $Sr(NO_3)_2$ became highly disordered when compressed. To study this pressure-induced transformation in more detail we used angle-dispersive x-ray diffraction (ADXD), which has a higher resolution than EDXD. The high pressure ADXD measurements on $Pb(NO_3)_2$ show that a disordered structure forms, but not an x-ray amorphous one. To probe further the pressure-induced transformation of the nitrates, we used Raman spectroscopy to study the reorientation of the nitrate ions. The transformation to this disordered state occurs via reorientation of the nitrate groups to multiple sites and movement of the metal ions away from their fcc crystal positions.

Although we began this work as part of an on-going research program to study pressure-induced amorphization, the results have a broader impact.[1–5] Specifically, we discuss the meaning of the phrase ''x-ray amorphous'' as applied to high pressure measurements. We also shed some light on the nature of the environments present in nitrate glasses.

The paper is divided into four sections: (1) experimental procedures, (2) experimental observations, (3) an interpretation of the transformation to the disordered state under compression, and (4) conclusions.

II. EXPERIMENTAL PROCEDURES

A summary of the experimental procedures used is presented here, while a detailed discussion of the techniques employed is discussed elsewhere.[6] A modified Merrill-Bassett style diamond anvil cell (DAC) was used to generate high pressures. Inconel gaskets preindented to 5/1000 in. with a 0.25 mm hole drilled in the indentation were used to contain the samples. A 4:1 methanol/ethanol mixture was used as a pressure transmitting fluid during all experiments. The samples were in powder form, typically ground to particles 100 mesh in size. The National Bureau of Standards (NBS) ruby calibration method was used to monitor the pressure. All high pressure Raman measurements and ADXD (angle-dispersive x-ray-diffraction) and EDXD (energy-dispersive x-ray-diffraction) measurements reported were reproducible.

The 514.5 nm line of a Spectra-Physics model 2020-5W argon ion laser was used for excitation of the Raman scattering effect; the scattered light was gathered at 160° to the incident exciting beam by a Spex 1403 double monochromator. Approximately 500 mW of power was incident on the sample for all experiments. Resolution was 4 cm^{-1} for all measurements.

The EDXD experiments were performed at CHESS (the Cornell High Energy Synchrotron Source) using a polychromatic x-ray beam and a Ge solid state detector.[7,8] Ed for all measurements was determined with a piece of gold foil, and is indicated in each figure caption. The same high pressure cells and experimental protocol were used as for the Raman measurements. The pressure was monitored by mixing 10% by volume gold powder (Alfa, 99.995%, grain size 1–3 μm) with the sample. The change in the (111) diffraction plane of gold was monitored; the pressure was then calculated using an equation of state.[9] All EDXD x-ray-diffraction peaks were fit with Gaussians using a nonlinear least squares algorithm.

Angle-dispersive x-ray-diffraction (ADXD) measurements were performed on two separate types of experimental apparatus at the National Synchrotron Light Source (NSLS). The first set of ADXD measurements were performed on the X17-B1 beam line at NSLS using 0.439 Å wavelength radiation. HR-IIIN Fuji image plates were placed ~210 mm from the diamond cell. This cell is similar to the one described for Raman and EDXD measurements, but was fitted with a rectangular pyramidal slot with included angles of 60° and 22°. The sample to plate distance was calibrated using the NIST α-Al_2O_3 (SRM 676) standard. The two-dimensional diffraction patterns on the plates were integrated using the methods described by Nelmes and co-workers.[10]

Diffractometer measurements were performed on the X7A beamline at NSLS using 0.696770 Å wavelength radiation.[11] Polychromatic radiation from the bending mag-

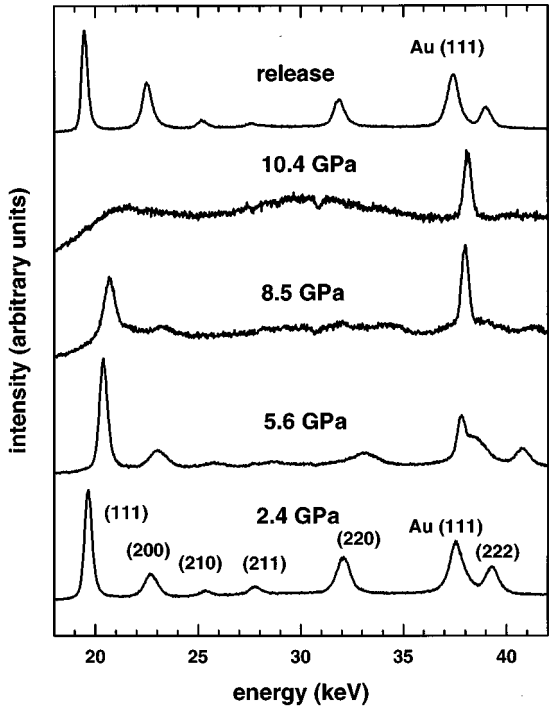

FIG. 1. Energy-dispersive x-ray-diffraction patterns of $Pb(NO_3)_2$ to 10.4 GPa. The spectra have been normalized to the intensity of the Au(111) peak ($Ed=88.035$ keV Å).

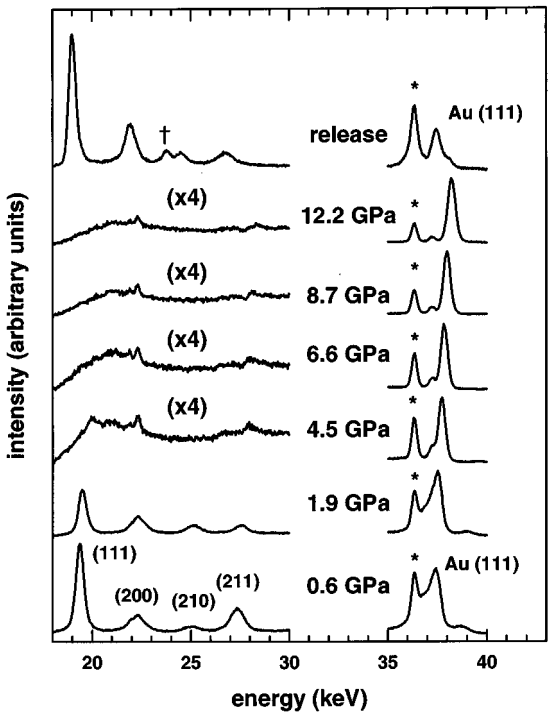

FIG. 2. Energy-dispersive x-ray-diffraction patterns of $Ba(NO_3)_2$ to 12.2 GPa. The spectra have been normalized to the intensity of the Au(111) peak. The feature labeled with an asterisk at ~36 keV is a barium x-ray fluorescence feature. The feature labeled with a cross may represent a diffraction plane consistent with a change to an orthorhombic form upon release of the pressure ($Ed=88.035$ keV Å).

net was monochromatized and focused in the horizontal plane with a triangular-shaped asymmetrically cut Si 220 silicon crystal bent to cylindrical curvature by point loading.[12] The crystal was set to a Bragg angle of 21.033° on the first axis to select ~0.7 Å radiation. A 10.0×0.2 mm^2 portion of the beam was focused at the sample position, 1.3 m away on the second axis. A 100 μm pinhole was placed immediately in front of the cell. A position sensitive detector (PSD) was used with a spatial resolution of ~0.03 mm. The PSD is a multiwire proportional device operated with 90% Kr and 10% CO_2 gas mixture at 4 bar.[13] The width of the active region of the detector is 10 mm, but only the central ±1° region of the detector is used to minimize parallax effects with step scans of 2° in $2q$. The detector was located about 45 cm from the sample, and was aligned optically with a telescope. CeO_2 (NBS reference material) on Kapton and aligned with the diffractometer center in a transmission geometry was used as a calibration standard. Samples were loaded as in the previous Raman experiments with a chip of ruby used for pressure determinations. Counting times of 10 min per 2° segment in $2q$ were used and the sample was rocked through ±0.5° to reduce preferred orientation effects.

The $Sr(NO_3)_2$, $Ba(NO_3)_2$, $Pb(NO_3)_2$, and $Cs(NO_3)_2$ crystalline samples were obtained from Johnson Matthey, Alfa Products (99.999%). The $CsPb(NO_3)_3$ glass was prepared by melting equimolar amounts of the constituents in a platinum crucible for 30 min and then splat quenching the melt between two brass plates.

III. EXPERIMENTAL OBSERVATIONS

We studied the effect of compression on the x-ray-diffraction patterns and the Raman spectra for the isostructural compounds $Pb(NO_3)_2$, $Ba(NO_3)_2$, and $Sr(NO_3)_2$. In general, EDXD experiments showed a disordered state was formed upon compression to 10.0 GPa for each of the compounds. A complete return to the crystalline state is observed when the pressure is released, albeit with considerable hysteresis as shown by energy-dispersive x-ray diffraction. To determine details of the transformation and whether the final state was truly x-ray amorphous we performed ADXD and diffractometer experiments on $Pb(NO_3)_2$. The results show that some diffraction peaks remained to 29.5 GPa, albeit greatly diminished in intensity and broadened. Additionally, high pressure Raman spectroscopy experiments showed the splitting of features, thus indicating that multiple nitrate environments were forming. The peak intensity in the Raman patterns also diminish greatly in intensity and the peaks broaden. The x-ray and Raman results taken together show that a disordered state is formed under compression, but not a totally x-ray amorphous one. Finally, we also measured the Raman spectra of amorphous $CsPb(NO_3)_3$ for comparison. We discuss the details of each measurement below.

X-ray diffraction: Energy dispersive

The effect of pressure on the powder energy-dispersive x-ray-diffraction (EDXD) patterns of the $Pb(NO_3)_2$ isomorphs shows that a highly disordered state forms at approximately 10.0 GPa (see Figs. 1–3). As the pressure is increased the diffraction pattern for each of these compounds shows a

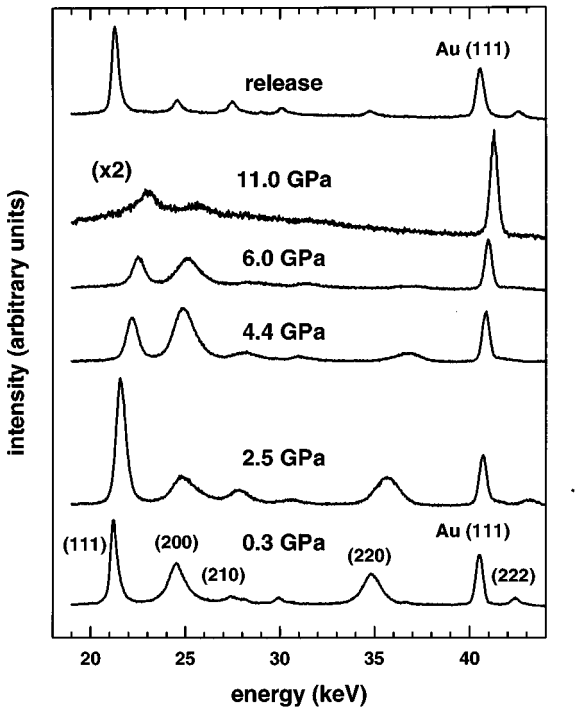

FIG. 3. Energy-dispersive x-ray-diffraction patterns of $Sr(NO_3)_2$ to 11 GPa. The spectra have been normalized to the intensity of the Au(111) peak ($Ed=95.37$ keV Å).

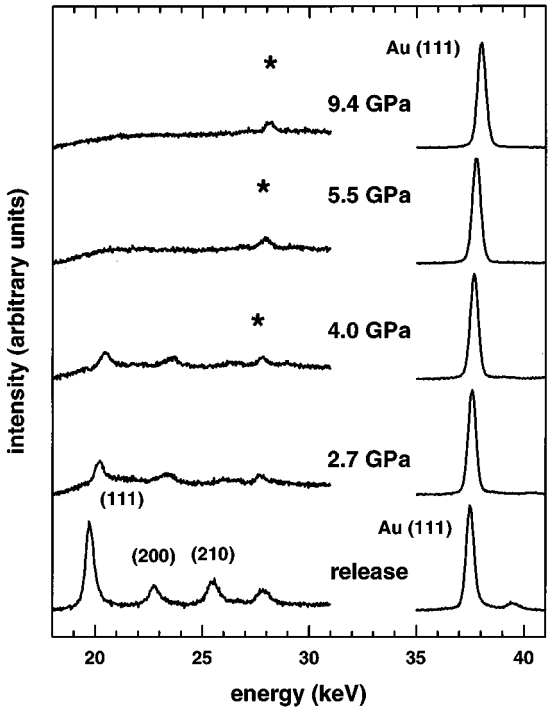

FIG. 4. Energy-dispersive x-ray-diffraction patterns of $Sr(NO_3)_2$ as the pressure is released. The spectra have been normalized to the intensity of the Au(111) peak. The feature indicated with an asterisk represents an artifact of the experiment ($Ed=88.035$ keV Å).

marked decrease in the d spacings and a loss of intensity; also the compounds undergo a volume change of approximately 18% in 10.0 GPa. The (111) diffraction peak in the x-ray pattern is the last feature retained; a broad hump characteristic of an amorphous state forms around this feature. Upon release of the pressure the crystalline diffraction peaks return, but with some loss of intensity. It required 24 h of relaxation to obtain the original x-ray-diffraction pattern for $Ba(NO_3)_2$, while those of $Sr(NO_3)_2$ and $Pb(NO_3)_2$ returned immediately upon release of the pressure. The reemergence of the x-ray-diffraction pattern occurs with considerable hysteresis in relation to the disappearance. It gradually disappears as the pressure increases, but the reemergence does not begin until the pressure has been released to approximately half of the maximum pressure of the experiment. The x-ray-diffraction pattern of $Sr(NO_3)_2$ was monitored upon decompression and did not reappear until approximately 4.0 GPa (see Figs. 3 and 4).

X-ray diffraction: Angle-dispersive and diffractometer measurements

The angle-dispersive x-ray-diffraction (ADXD) patterns for $Pb(NO_3)_2$ are presented in Figs. 5 and 6. The results from the ADXD experiments on both types of apparatus at NSLS were comparable. The result shows that the diffraction peaks shift at a rate comparable to that observed in the EDXD experiments, but features not apparent in the EDXD pattern appear: above 9.5 GPa crystalline peaks remain indicating a disordered state, but not an amorphous state. The main feature remaining is the remnant of the (111) diffraction peak. Just as in the EDXD experiments there is a precipitous decline in intensity, and broadening of the width of diffraction peaks, but the sample contains remnants of crystallinity to the highest pressure attained, 29.5 GPa. Shown in Fig. 6 is the ADXD diffraction pattern at a pressure of 12.9 GPa. One can clearly see that a degree of crystallinity that remains.

We attempted to fit this diffraction pattern to that of orthorombic $Pb(NO_3)_2$ (see discussion below). Although the pattern in Fig. 6 is reminiscent of the orthorombic phase, it cannot be fit to it. Note particularly the peak around $2\theta=6.1°$. This is a single peak in the orthorombic lead nitrate phase, but is split into two peaks here. Combing this observation with the raman spectra described below suggest strongly looking for a lower symmetry version of the orthorombic lead nitrate structure. We were unable to unambiguously index this pattern to a cell; a larger set of peaks in reciprocal lattice space are needed to find the precise phase. Note, though, that the spectra do clearly indicate a lowering of symmetry of the ambient pressure, cubic structure of $Pb(NO_3)_2$.

Raman measurements

The effect of compression on the Raman spectra of $Pb(NO_3)_2$, $Ba(NO_3)_2$, and $Sr(NO_3)_2$ are presented in Figs. 7–9. Understanding the change with pressure of these spectra is crucial in understanding how the disordered state forms. We monitored three regions of the Raman spectra: (1) the symmetric stretch of the NO_3^- ion ($\sim$1050 cm^{-1}), (2) the in-plane bending mode of the NO_3^- ion ($\sim$730 cm^{-1}), and (3) the lattice modes (100–250 cm^{-1}).[14–16] Of particular interest is the nondegenerate (A_g) symmetric stretch of the NO_3^- ion. This stretch is especially sensitive to

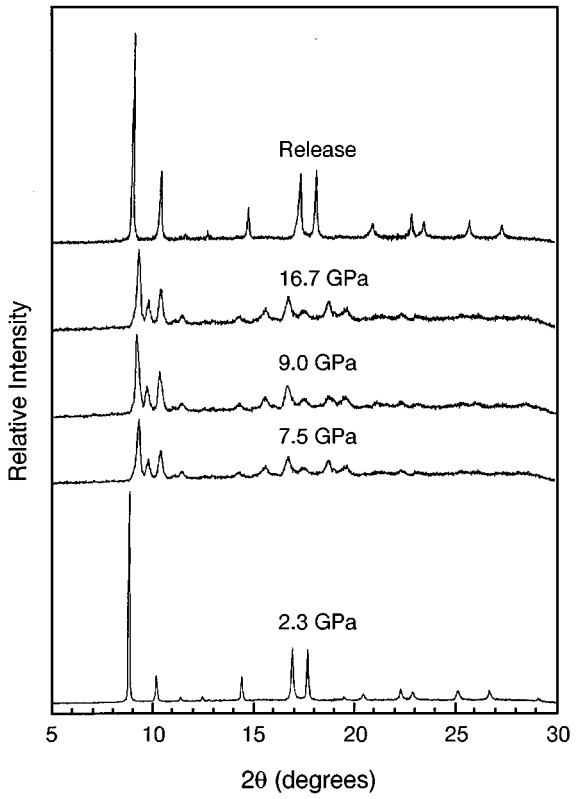

FIG. 5. Diffractometer x-ray-diffraction patterns of $Pb(NO_3)_2$ to 16.7 GPa.

the onset of disorder, while the x-ray-diffraction pattern will give only an average structure.[14]

In general, compression causes a splitting of the symmetric stretch into multiple features, a splitting of the in-plane bending modes into two bands approximately 20 cm^{-1} apart, which are composed of multiple peaks, and a loss of intensity of these modes and the lattice modes. In addition to the splitting seen, the symmetric stretch also blue shifts under compression, while the in-plane bending mode does not shift appreciably after splitting. In addition, all the features exhibit a precipitous decline in intensity which is characteristic of a disordered state.[17] In the figures the intensity scale varies from spectrum to spectrum; the scale becomes elongated as the pressure increases. The amount of noise in a spectrum is an indicator of its weakness relative to other spectra within a pressure run. If the high and low pressure spectra were plotted on the same scales, then the features in the high pressure spectra would not be visible. The specific behavior for each compound is as follows.

Raman measurements: $Pb(NO_3)_2$

The high pressure Raman spectra of $Pb(NO_3)_2$ are presented in Fig. 7. Compression to 5.3 GPa causes the symmetric stretch to split into two distinct features, with the new feature at lower energy. The in-plane bending mode splits into two bands consisting of multiple components, and the lattice modes present between 100 and 250 cm^{-1} blue shift and lose intensity. In addition, a Raman band at 815 cm^{-1} becomes active. By 9.2 GPa the symmetric stretch is split by 8 cm^{-1}, the bending mode has continued to blue shift and remains split, and the lattice modes can no longer be observed. Compression to 13.0 GPa results in additional blue shifting of the remaining modes and lose of intensity. Upon release of the pressure the Raman spectrum characteristic of the initial crystalline state returns.

Raman measurements: $Ba(NO_3)_2$

The high pressure Raman spectra of $Ba(NO_3)_2$ are presented in Fig. 8. Compression to 5.9 GPa causes the symmetric stretch to split into at least four distinct features, with the new features at lower energy. The in-plane bending mode splits into two bands consisting of multiple components, and the lattice modes present between 100 and 250 cm^{-1} blue shift and lose intensity. By 10.0 GPa the symmetric stretch has merged into one larger feature with a full width at half maximum (FWHM) of approximately 50 cm^{-1}, the bending mode has continued to blue shift, remains split and loses intensity, and the lattice modes can no longer be observed. Compression to 13.0 GPa results in additional blue shifting of the remaining modes and lose of intensity. Upon release of the pressure the Raman spectrum characteristic of the initial crystalline state returns.

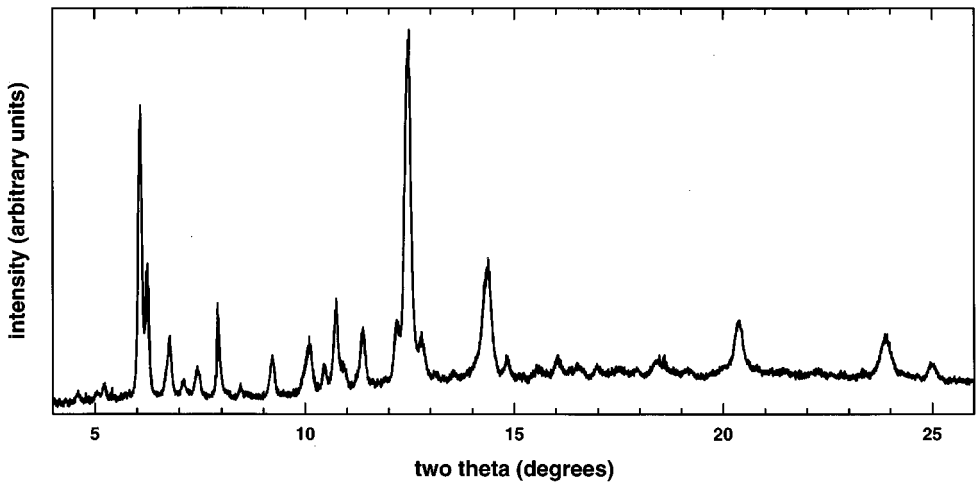

FIG. 6. Angle-dispersive x-ray-diffraction (ADXD) pattern of $Pb(NO_3)_2$ at 12.9 GPa.

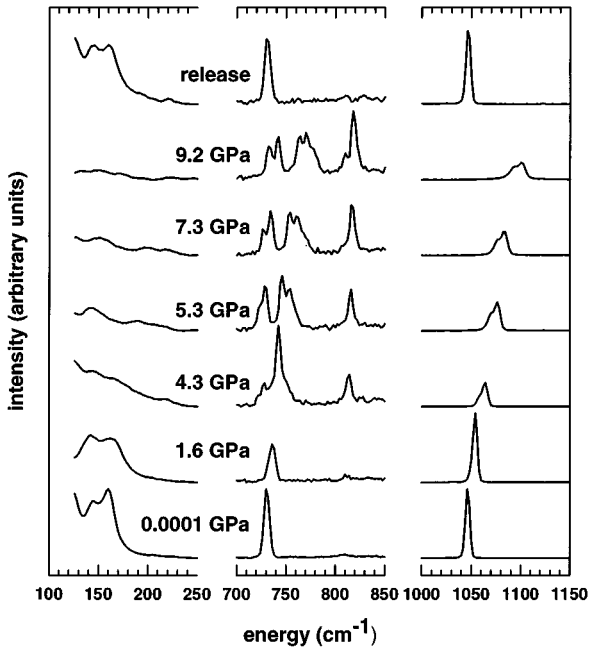

FIG. 7. The effect of pressure on the Raman spectrum of $Pb(NO_3)_2$. On an absolute scale the intensity of 1000–1150 cm^{-1} region is ~10 times more intense than the 700–850 cm^{-1} region, and the 700–850 cm^{-1} region is ~2.5 times more intense than the 100–250 cm^{-1} region. The scales of the intensity axes are expanded for all the regions. If the high and low pressure spectra were plotted on the same scales, then the features in the high pressure spectra would not be visible.

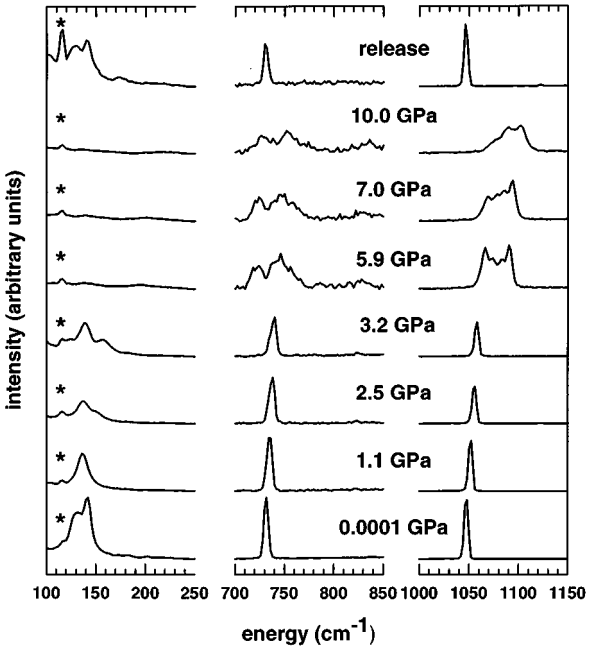

FIG. 8. The effect of pressure on the Raman spectrum of $Ba(NO_3)_2$. On an absolute scale the intensity of 1000–1150 cm^{-1} region is ~10 times more intense than the 700–850 cm^{-1} region, and the 700–850 cm^{-1} region is ~2.5 times more intense than the 100–250 cm^{-1} region. The scales of the intensity axes are expanded for all the regions. If the high and low pressure spectra were plotted on the same scales, then the features in the high pressure spectra would not be visible. The feature labeled with an asterisk represents a plasma line, which is an artifact of the experiment.

Raman measurements: $Sr(NO_3)_2$

The high pressure Raman spectra of $Sr(NO_3)_2$ are presented in Fig. 9. Compression to 6.4 GPa causes the symmetric stretch of the NO_3^- ion to split into two features, with the new feature at lower energy. The new feature is much weaker and the splitting much less than that seen in the previous compounds. The in-plane bending mode splits into two bands consisting of multiple components, and the lattice modes present between 100 and 250 cm^{-1} blue shift and lose intensity. Compression to 13.4 GPa causes the symmetric stretch to continue blue shifting, the bending mode has continued to blue shift and remains split, and the lattice modes can no longer be observed while the others have also lost intensity. Upon release of the pressure the Raman spectrum characteristic of the initial crystalline state returns.

Raman measurements: Amorphous $CsPb(NO_3)_3$

Amorphous $CsPb(NO_3)_3$ is chosen for comparison with the pressure-induced disordered state of $Pb(NO_3)_2$, because $Pb(NO_3)_2$ does not form a melt quenched glass by itself. The Raman spectra of glassy $CsPb(NO_3)_3$ consists of a broad feature in the 1045 cm^{-1} region, with a FWHM of 15 cm^{-1}, a broad band centered around 720 cm^{-1} consisting of two features each with approximately a 15 cm^{-1} FWHM, no observable lattice modes, and a feature at 815 cm^{-1} (Fig. 10). The Raman spectrum of $Pb(NO_3)_2$ at 13.0 GPa matches that of glassy $CsPb(NO_3)_3$ in terms of band splittings and the FWHM. However, the position of the Raman bands for $Pb(NO_3)_2$ occur at higher wave numbers, because of compression of the nitrate ion.

IV. INTERPRETATION OF THE PRESSURE-INDUCED TRANSFORMATION

To interpret the effect of compression on the three nitrates compounds, we must first examine their crystal structures. The structures of lead, barium, and strontium nitrate are isomorphous to $Ca(NO_3)_2$ and a high temperature (160 °C) form of $Cd(NO_3)_2$.[18–25] The crystal structure $[Pa3(T_h^6)]$ consists of a cubic face-centered arrangement of metal (M^{+2}) ions with nitrate groups in between. The nitrogen atoms are on the threefold axes and the metal ions are coordinated by twelve oxygen atoms in the shape of a distorted cubocathedron. There are four NO_3 units per unit cell, with one crystallographically distinct nitrate group and one crystallographically distinct M^{+2} cation in the structure. The three compounds studied in this work have similar sized unit cells; the major difference among the structures is the height of the NO_3 pyramid.

We will discuss the transformation of the $Pb(NO_3)_2$ crystal, but the arguments apply equally to $Ba(NO_3)_2$ and $Sr(NO_3)_2$. The application of high pressure causes compression, distortion, and reorientation of the NO_3^- groups lying above and below the (111) plane, thus breaking the cubic symmetry. The reorientation of the nitrate groups results in multiple sites, which are manifest in the splittings observed in the Raman spectra for the symmetric and out-of-plane

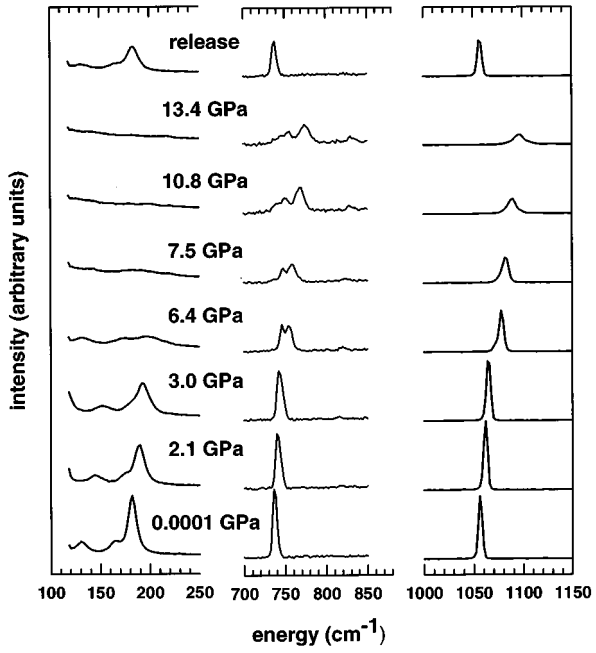

FIG. 9. The effect of pressure on the Raman spectrum of $Sr(NO_3)_2$. On an absolute scale the intensity of 1000–1150 cm^{-1} region is ~10 times more intense than the 700–850 cm^{-1} region, and the 700–850 cm^{-1} region is ~2.5 times more intense than the 100–250 cm^{-1} region. The scales of the intensity axes are expanded for all the regions. If the high and low pressure spectra were plotted on the same scales, then the features in the high pressure spectra would not be visible.

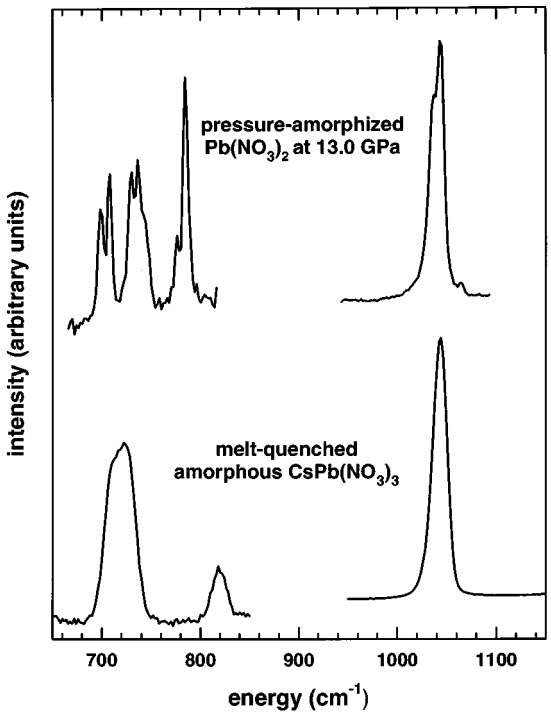

FIG. 10. Comparison between the Raman spectrum of pressure amorphized $Pb(NO_3)_2$ melt-quenched amorphous $CsPb(NO_3)_3$. The shifts of the features in the pressure-amorphized sample have been adjusted for compression.

bending modes of the nitrate ion. As the pressure continues to increase the nitrate ions compress and continue to reorient, eventually forcing the M^{+2} ions away from their crystal positions resulting in a disordered state as reflected in the x-ray-diffraction patterns observed (see Fig. 11). Support for this interpretation is drawn, in addition to our high pressure data, from four general areas: (a) Raman studies of $Cd(NO_3)_2$, (b) high pressure x-ray and Raman data for $CaCO_3$, (c) experimental studies of other nitrates, and (d) theoretical work on the Raman spectra of nitrate crystals under various conditions.

The high pressure Raman spectra of $Pb(NO_3)_2$ and the low temperature Raman spectra of $Pb(NO_3)_2$, $Cd(NO_3)_2$, and $Ca(NO_3)_2$ show many similarities. The low temperature Raman spectra of $Pb(NO_3)_2$ resemble the high pressure spectra in terms of band splittings.[23] A $Cd(NO_3)_2$ isomorph exists in a low temperature (160 °C) orthorhombic form with unit cell parameters doubled in the *b* direction, and two crystallographically distinct types of NO_3^- groups and M^{+2} cations. The orthorhombic form has the cations slightly displaced from their fcc sites, and the nitrate ions rotated in their plane from their positions in the cubic form.[26,27] $Ca(NO_3)_2$ also appears to transform to this orthorhombic structure at 80 K. The Raman spectra of the orthorhombic phase for both of these compounds indicate the presence of four crystallographically distinct sites for the nitrate ion.[28] The Raman spectra for $Cd(NO_3)_2$ at 77 K exhibit multiple bands in the symmetric and in-plane bending modes similar to our highest pressure Raman spectra for $Pb(NO_3)_2$. The symmetric stretching modes show a multiplet structure with four bands arranged in two sets of two features at 1068.8 and 1070 cm^{-1}. Isotopic studies indicate the four bands are due to four sets of nonequivalent NO_3^- ions in the $Cd(NO_3)_2$ structure. The in-plane bending mode in the 700–800 cm^{-1} region is also split into multiple bands due to a lifting of the degeneracy, resulting in two types of vibrations. It has been suggested that this phase change occurs because the NO_3^- groups rotate or a distortion in the structure is caused by a change in interatomic distances within the structure. Some combination of both mechanisms is the most probable

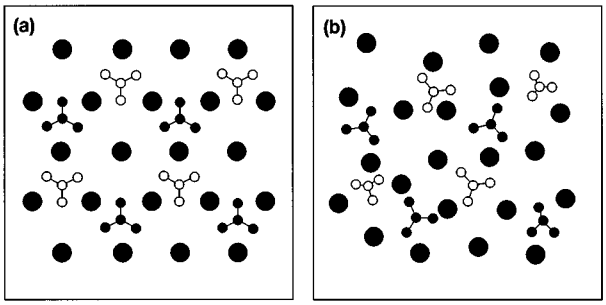

FIG. 11. View of the (111) plane of lead nitrate (a) before disordering and (b) after disordering. This shows the proposed changes to the nitrate ions and lead atoms. The large black dots are the lead atoms. The dark nitrate ions lie 0.27 Å below the plane of lead atoms and the lighter nitrate ions lie 0.27 Å above the plane of lead atoms.

outcome.[28] In addition, the $Cd(NO_3)_2$ orthorhombic form is more dense than the cubic form, 2.69 vs 2.65 g/cm^3. Thus the transformation to a more dense state would be consistent with the application of pressure.

Similarities between our data and the high pressure response of $CaCO_3$ also exist, lending further support to our interpretation of our results. Specifically, changes in the Raman spectra of $CaCO_3$ under compression are similar in nature to the changes we observed in the Raman spectra of the nitrates under compression. At ambient temperature $CaCO_3$ undergoes the transformation calcite(I)-calcite(II)-calcite(III), at 1.5 and 1.9 GPa, respectively. Merrill and Bassett showed using x-ray diffraction that the calcite(I)-calcite(II) transformation occurs under pressure via rotation of carbonate ions by 11° and displacement of alternate planes of calcium atoms along the *c* axis.[29] Raman spectra documenting this transformation show a splitting of the nondegenerate symmetric CO_3^- stretch at 1070 cm^{-1}, with the new feature growing in at lower energy. The doubly degenerate out of plane bending mode of CO_3^- at ~700 cm^{-1} splits into two distinct bands, one of which clearly consists of multiple features.[30,31]

A number of other studies have found evidence for the presence of multiple sites in monovalent and divalent nitrate crystals. Multiplet structures in the symmetric stretching region have been observed for a number of these ionic salts. Raman spectra similar to those we observed for $Pb(NO_3)_2$ isomorphs under compression are observed for those compounds.[32,33] The presence of a Raman feature at slightly lower energy than the symmetric stretch could not be assigned for a number of salts based on their crystal structure. Therefore, Badr *et al.* assigned the lower energy component to an ''energetically'' distinguishable alternate structure, on the basis of its enhanced intensity with increasing temperature.[34] Single crystal studies of $Ag(NO_3)$, KNO_3(II), and $TlNO_3$ support the view and suggest the second sites are Frenkel type defects which result from alternate orientations of the NO_3^- ions.[32,35]

Lastly, theoretical studies of Karpov and Shultin on $NaNO_3$ suggest the symmetric stretch in the Raman spectra of $NaNO_3$ would consist of a number of components depending on the various local fields of orientational nearest neighbors.[36,37] The $NaNO_3$ crystal has the calcite structure at room temperature, and as the temperature is increased the disordered structure is influenced by the appearance of the alternate aragonite orientation of the nitrate ion. As the temperature rises the nitrate ions reorient to their configuration in the aragonite structure. The presence of aragonite nearest neighbors in conjunction with calcite neighbors for a given NO_3^- ion result in eight bands appearing in the symmetric stretch as each NO_3^- ion has three NO_3^- ion neighbors in either a calcite or aragonite orientation. The calculated Raman spectra agreed reasonably well with the literature for the symmetric stretch. Therefore one would expect multiple bands to occur in the symmetric stretch of $Pb(NO_3)_2$ under compression due to similar interactions as reorientation of the nitrate ion occurs.

V. CONCLUSIONS

We have presented in this work x-ray-diffraction measurements of $Pb(NO_3)_2$, $Ba(NO_3)_2$, and $Sr(NO_3)_2$ under compression. The results show the reversible, pressure-induced transformation to a disordered structure. We used Raman spectra, obtained under compression, to suggest that the transformations occur because the nitrate groups compress, distort, and rotate. There are several broad conclusions we draw in this section. The first concerns the terms ''x-ray amorphous'' as used in pressure-induced amorphization. Second, we suggest the results reported here yield insight about the use of Raman spectroscopy to determine the atomic structure of nitrate-based glasses.

X-ray amorphous. The reader will notice that using the high pressure EDXD measurements led one to conclude that the nitrate crystals were ''x-ray amorphous'' at high pressures, while the results from the diffractometers show the crystals are highly distorted. Thus, one of our key conclusions, then, is that the terms ''x-ray amorphous'' must be qualified with a description of the technique used. (Note, though, that some samples that become amorphous by compression are truly amorphous; for example, α quartz.[38,39])

Glass structure. There is a debate about whether Raman spectroscopy can delineate among the nitrate environments present in metal-nitrate based glasses. Two views have been expressed concerning the structure of nitrate glasses, and more specifically the distribution of cations in the material. The first viewpoint suggests that the Raman spectra for both glassy and molten nitrates are largely independent of the detailed geometry of the model.[16] Furkawa *et al.* show that a tremendous range of perturbing forces will produce essentially the same details of band broadening and splitting as seen in the Raman spectra of a nitrate glass. They conclude that a continuum of nitrate environments exist, which are indistinguishable by vibrational spectroscopy, even though moderately sharp spectra exist with well defined band splittings. The opposite view concludes that certain bands in the glassy nitrate spectrum are associated with a particular cation or a mixture of both cations, resulting in a nonrandom arrangement of cations.[40–42] Thus there are specific anion (nitrate) sites associated with each type of cation. Also, by studying $M(II)(NO_3)_2/NH_4NO_3$ glasses and $CdTl(NO_3)_3$ glasses, Carrick and co-workers showed that similarities exist between the crystalline and glassy nitrate environments.

We believe that Raman spectroscopy *can* be used to differentiate among a number of distinguishable nitrate environments in the amorphous phase. The nitrate and cation environments present in the distorted crystals at high pressure are very similar to those present in the nitrate glasses. Comparisons between the high pressure $Pb(NO_3)_2$ phase and glassy $CsPb(NO_3)_3$ at ambient pressure show similarities in form and structure, specifically noting the region at ~1045 cm^{-1} for the $Pb(NO_3)_2$ phase. Multiple, sharp features corresponding to specific nitrate environments are observed to be derived from a single nitrate type under compression. These are remarkably similar to those of the amorphous nitrate. We are able to create highly distorted nitrate crystals that exhibit Raman features very similar to those of nitrate glasses. Thus these results suggest that vibrational spectroscopy can be used to delineate different but specific types of nitrate environments in glassy nitrates in accord with the work of Carrick *et al.*[42]

ACKNOWLEDGMENTS

This work was supported by the Division of Material Sciences, Office of Basic Energy Sciences, Department of Energy, under Contract No. DE-FG02-92ER45474. We thank Dr. Keith Brister and the staff at CHESS for their assistance with the high pressure EDXD experiments. We also thank Dr. Mark Rivers, Dr. Nancy Lazarz, Dr. David Cox, and the staff at NSLS for their help with the ADXD experiments. Finally, we thank Kenneth Meyer and Paul Klabnik at Carnegie Mellon University for their technical assistance.

*Author to whom correspondence should be addressed.

[1] Y. Fujii, M. Kowaka, and A. Onodera, J. Phys. C **18**, 789 (1985).
[2] M. B. Kruger and R. Jeanloz, Science **249**, 647 (1990).
[3] R. J. Hemley, in *High-Pressure Research in Mineral Physics*, edited by M. H. Manghnani and Y. Syono (Terra Scientific, Tokyo, 1987), p. 347.
[4] G. C. Serghiou, R. R. Winters, and W. S. Hammack, Phys. Rev. Lett. **68**, 3311 (1992).
[5] R. R. Winters and W. S. Hammack, Science **260**, 202 (1993).
[6] G. C. Serghiou and W. S. Hammack, J. Chem. Phys. **95**, 5212 (1991).
[7] M. A. Baublitz, V. Arnold, and A. L. Ruoff, Rev. Sci. Instrum. **52**, 1616 (1981).
[8] K. Brister, Y. K. Vohra, and A. L. Ruoff, Rev. Sci. Instrum. **57**, 2560 (1986).
[9] D. L. Heinz and R. Jeanloz, J. Appl. Phys. **55**, 885 (1984).
[10] R. J. Nelmes, P. D. Hatton, M. I. McMahon, R. O. Pilz, J. Crain, R. J. Cernik, and G. Bushnell-Wye, Rev. Sci. Instrum. **63**, 1039 (1992).
[11] A. P. Jephcoat, L. W. Finger, and D. E. Cox, High Press. Res. **8**, 667 (1992).
[12] M. Lemonnier, R. Fourme, F. Rousseaux, and R. Kahn, Nucl. Instrum. Methods **152**, 173 (1978).
[13] R. A. Boie, J. Fischer, Y. Inagaki, F. C. Merritt, V. Radeka, L. C. Rogers, and D. M. Xi, Nucl. Instrum. Methods **201**, 93 (1982).
[14] M. H. Brooker and D. E. Irish, J. Chem. Phys. **53**, 1083 (1970).
[15] I. Nakagawa and J. L. Walter, J. Chem. Phys. **51**, 1389 (1969).
[16] T. Furkawa, S. A. Bawer, and W. B. White, J. Chem. Phys. **69**, 2639 (1978).
[17] R. Shuker and R. W. Gammon, Phys. Rev. Lett. **25**, 222 (1970).
[18] H. Nowotny and G. Heger, Acta Crystallogr. C **39**, 952 (1983).
[19] H. Nowotny and G. Heger, Acta Crystallogr. C **42**, 133 (1986).
[20] W. C. Hamilton, Acta Crystallogr. **10**, 103 (1957).
[21] R. W. Wyckoff, *Crystal Structures* (Interscience, New York, 1963), Vol. 2.
[22] V. R. Birnstock, Z. Kristallogr. **124**, 310 (1967).
[23] M. H. Brooker and J. B. Bates, Spectrochim. Acta, Part A **29**, 439 (1973).
[24] R. A. Santos, P. Tang, W.-J. Chein, S. Kwan, and G. S. Harbison, J. Phys. Chem. **94**, 2717 (1990).
[25] M. H. Brooker, Phys. Status Solidi A **157**, 167 (1990).
[26] M. Louer, D. Louer, and D. Grandjean, J. Solid State Chem. **17**, 231 (1976).
[27] D. Weigel, B. Imelik, and M. Prettre, Mem. Pres. Soc. Chim. **25**, 2600 (1964).
[28] M. H. Brooker, Spectrochim. Acta, Part A **32**, 369 (1976).
[29] L. Merrill and W. A. Bassett, Acta Crystallogr. B **31**, 343 (1975).
[30] M. Y. Fong and M. Nicol, J. Chem. Phys. **54**, 579 (1971).
[31] L.-G. Liu and T. P. Mernagh, Am. Mineral. **75**, 801 (1990).
[32] M. H. Brooker, J. Chem. Phys. **68**, 67 (1978).
[33] Z. X. Shen and W. F. Sherman, J. Mol. Struct. **247**, 397 (1991).
[34] Y. A.-K. Badr, S. V. Karpov, and A. A. Shultin, Sov. Phys. Solid State **16**, 1515 (1975).
[35] C.-H. Huang and M. H. Brooker, Spectrochim. Acta, Part A **32**, 1715 (1976).
[36] S. V. Karpov and A. A. Shultin, Sov. Phys. Solid State **18**, 421 (1976).
[37] F. C. Kracek, J. Am. Chem. Soc. **53**, 2609 (1931).
[38] R. R. Winters, A. Garg, and W. S. Hammack, Phys. Rev. Lett. **69**, 3751 (1992).
[39] K. J. Kingma, C. Meade, R. J. Hemley, H.-k. Mao, and D. Veblen, Science **259**, 569 (1993).
[40] D. W. James and M. T. Carrick, Aust. J. Chem. **39**, 325 (1986).
[41] W. H. Leong and D. W. James, Aust. J. Chem. **36**, 235 (1983).
[42] M. T. Carrick, D. W. Jones, and W. H. Leong, Aust. J. Chem. **36**, 223 (1983).